EFFECT OF FRICTION ON MOTION OF A PISTON DRIVEN BY COMBUSTION PRODUCTS

V. A. Poselevich, N. N. Pilyugin, and S. Yu. Chernyavskii

UDC 531.44:531.57

In recent years the two-stage light gas ballistic apparatus with deformable plastic pistons has become widely used in experimental aerodynamics. The existing methods of calculating such devices either completely neglect friction of the piston on the channel wall [1-3] or use a schematization of the frictional forces [4-6], which does not have a satisfactory physical basis. In a number of studies [7, 8] the friction force was considered constant, and its value was specified not from physical considerations, but to produce the best agreement between calculated and experimental values of object velocity or driving gas pressure. Since friction is such a significant factor, its proper consideration in calculating piston motion parameters requires special study. In this connection, it is useful to consider the operation of only the first stage of the ballistic apparatus, which sets the piston in motion. Below we will consider the problem of the internal ballistics of a one-stage powder-driven apparatus in the column channel of which a piston made of polymer material moves, experiencing friction. The friction model is constructed on the basis of a series of experiments on the slow forcing of polymer specimens compressed in the longitudinal direction through a steel channel. An experimental study was made of the relationship between the gunpowder gas pressure and time within a constant volume chamber, allowing establishment of the true powder-burning law, and its deviation from the geometric law of [9]. Calculated and experimental values of maximum gas pressure and muzzle velocity of a polyethylene piston are compared.

1. Since no information is available on the character of the friction between solid polymers and a metallic surface at contact pressures of the order of 10^8 N/m^2, a series of experiments was performed by forcing longitudinally compressed polymer specimens through a cylindrical steel channel. Friction forces were measured at very low specimen velocities (10^{-4}–10^{-3} m/sec). The channel surface was finished to a point where the height of nonuniformities did not exceed $1.5 \cdot 10^{-6}$ m. Uncertainty in measurement of the specimen axial compression force F_0 and the friction force F did not exceed 25 and 10 N, respectively. The specimens were prepared from high pressure polyethylene and caprolon. Experiments were performed with specimens of various lengths l from $0.5 \cdot 10^{-2} \pm 10^{-5}$ to $4.0 \cdot 10^{-2} \pm 10^{-5}$ m in channels with diameters d from $0.8 \cdot 10^{-2} \pm 10^{-5}$ to $3.4 \cdot 10^{-2} \pm 10^{-5}$ m.

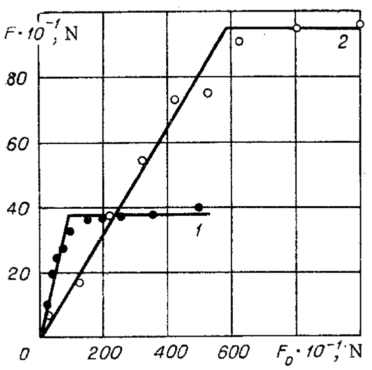

Fig. 1

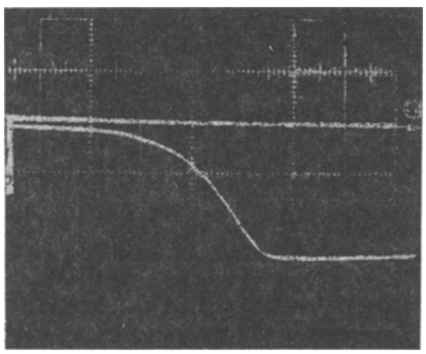

Fig. 2

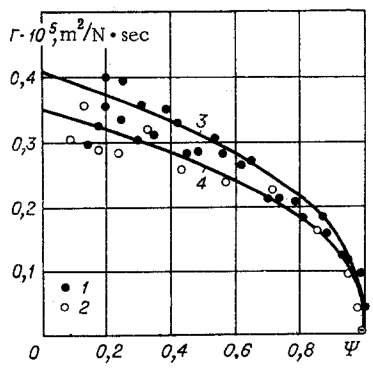

Fig. 3

Moscow. Translated from Zhurnal Prikladnoi Mekhaniki i Tekhnicheskoi Fiziki, No. 5, pp. 73-80, September-October, 1978. Original article submitted September 6, 1977.

TABLE 1

No.	Piston friction on column channel wall	Combustion law	ω, N	$v^*\cdot 10^{-3}$, m/sec	$p^*\cdot 10^{-8}$, N/m^2
1	Considered	Actual	0,98 1,22	0,841 0,913	1,27 2,13
2	Absent	Actual	0,98 1,22	1,18 1,38	0,66 1,05
3	Considered	Geometric, $I=0.215\cdot 10^6$ N·sec/m^2	0,98 1,22	0,961 1,07	1,55 2,64
4	Experiment		0,98 1,22	0,97 1,12	1,52 2,07

Figure 1 shows typical experimental curves of $F=F(F_0)$ at $l/d=1.78$ (curve 1, polyethylene; curve 2, caprolon). Two characteristic regions can be seen in the $F(F_0)$ curves. In the first of these F increases in proportion to F_0, while in the second F remains constant. As F_0 was decreased, the $F(F_0)$ curves had the same form as found with increasing F_0. Additional measurements showed that the yield point for expansion also comprised $1.1\cdot 10^7$ N·m^2 for polyethylene and $9.2\cdot 10^7$ N·m^2 for caprolon.

2. In calculating the motion, wave processes in the piston body may be ignored. Due to the low compressibility of polymer materials [10], we will assume the piston to be incompressible. This means that all of its elements move with identical velocity. Assuming that normal stresses in the piston cross sections are distributed uniformly, we find the equation of its motion in the form

$$\frac{d\sigma}{dx}+\frac{4\tau}{d}\frac{v}{|v|}+\rho a=0, \tag{2.1}$$

where ρ is the density of the piston material; v and a, its velocity and acceleration; σ, normal axial stress; x, axial coordinate; d, piston diameter. The boundary conditions for Eq. (2.1) have the form

$$\sigma(x_1,\ t)=p_1(t),\ \sigma(x_2,\ t)=p_2(t) \tag{2.2}$$

(x_1 and $x_2=x_1+l$, coordinates of the piston face sections; p_1 and p_2, pressures at the faces; l, piston length). For each moment of time Eq. (2.1) with consideration of Eq. (2.2) determines the distribution of σ over piston length. From the additional assumption of elastic deformability of the piston material together with its incompressibility, it follows that the piston pressure on the channel wall in each section coincides with the corresponding axial normal stress σ.

The results of friction force measurements permit the assumption that for $\sigma < p_c$ the dry (Coulomb) friction law

$$\tau=k\sigma \tag{2.3}$$

is valid, where k is the friction coefficient, while for $\sigma \geq p_c$ the friction stress remains constant

$$\tau=\tau_c=kp_c. \tag{2.4}$$

For $p_i < p_c$ (i = 1, 2) Eq. (2.3) is fulfilled over the entire lateral surface of the piston, and the solutions of Eq. (2.1) has the form

$$\sigma=-\frac{\rho a}{b}+(p_1-p_2)\frac{\exp(-bx)}{\exp(-bx_1)-\exp(-bx_2)},\quad b=\frac{4kv}{d\,|v|}, \tag{2.5}$$

while the piston acceleration is given by

$$a=\frac{b}{\rho}\,\frac{p_1\exp(-bl)-p_2}{1-\exp(-bl)}. \tag{2.6}$$

Integrating the stress τ over the lateral piston surface, for the net friction force F we find

$$F=\frac{\pi d^2}{4}\left[p_1-p_2-bl\,\frac{p_1\exp(-bl)-p_2}{1-\exp(-bl)}\right]\frac{v}{|v|}. \tag{2.7}$$

In the case where $bl \ll 1$,

$$F = \pi dlk \frac{p_1 + p_2}{2} \frac{v}{|v|}.$$

For $p_i \geq p_c$ ($i = 1, 2$) the friction stress is constant and equal to τ_c over the entire lateral surface of the piston. In this case

$$\sigma = p_1 - \left(\frac{4\tau_c}{d} \frac{v}{|v|} + \rho a\right)(x - x_1), \qquad (2.8)$$

$$a = \frac{p_1 - p_2}{\rho l} - \frac{4\tau_c}{\rho d} \frac{v}{|v|},$$

and the friction force is given by the formula

$$F = \pi dl\tau_c. \qquad (2.9)$$

If $p_1 \geq p_c$, and $p_2 < p_c$, on the portion of the lateral piston surface where $x_1 \leq x \leq x_c$ Eq. (2.4) is satisfied, while in the remaining area ($x_c < x \leq x_2$), Eq. (2.3) is satisfied. Then from Eqs. (2.5), (2.8) we have a transcendental equation for a

$$\ln \frac{p_2 + \frac{\rho a}{b}}{p_c + \frac{\rho a}{b}} - \frac{p_1 - p_c}{p_c + \frac{\rho a}{b}} + bl = 0, \qquad (2.10)$$

and to determine the coordinate of the point where the friction laws change, we have the formula

$$x_c = x_1 + (p_1 - p_c)\left(\frac{4\tau_c}{d} \frac{v}{|v|} + \rho a\right)^{-1}.$$

For $p_1 < p_c$ and $p_2 \geq p_c$, we obtain the analogous relationships

$$\ln \frac{p_c + \frac{\rho a}{b}}{p_1 + \frac{\rho a}{b}} + \frac{p_2 + p_c}{p_c + \frac{\rho a}{b}} + bl = 0.$$

We note that the formulas for acceleration obtained above lose their sense for $v = 0$ and $|p_1 - p_2| \frac{\pi d^2}{4} \leqslant F$ and must be replaced by the condition $a = 0$.

In processing the experimental data presented in Sec. 1, Eqs. (2.7), (2.9) were used with consideration of the condition $a = 0$ and the obvious relationships

$$p_1 = \frac{4(F + F_0)}{\pi d^2}, \quad p_2 = \frac{4F_0}{\pi d^2}.$$

Then the first section of the $F = F(F_0)$ curve is described by the equation

$$F = F_0\left(\exp \frac{4kl}{d} - 1\right). \qquad (2.11)$$

In the second section, where the friction force is constant,

$$F = \pi dl\tau_c. \qquad (2.12)$$

By processing the experimental data with Eqs. (2.11), (2.12) the following values were obtained for the constants defining the friction: polyethylene, $k = 0.054$, $p_c = 0.19 \cdot 10^8$ N/m², $\tau_c = 1.36 \cdot 10^6$ H/m²; caprolon, $k = 0.025$, $p_c = 1.17 \times 10^8$ N/m², $\tau_c = 3.1 \cdot 10^6$ N/m². For each specimen the uncertainty in determining the coefficient of friction k and the value of p_c did not exceed 10%, while the uncertainty in τ_c was less than 2.5%. Scattering in k, p_c, and τ_c values for various polyethylene specimens did not exceed 10% on the average, at a confidence level of 0.9. For the caprolon specimens the k value scattering was also 10%, while p_c and τ_c scattering reached 15%.

The results obtained confirmed the validity of Grigoryan's hypothesis [11] that friction stress at the contact point of solid bodies (rocks, soils, snow avalanches, glaciers, etc.) is limited by the shear strength of the weaker material. As follows from Fig. 1, for pressures exceeding the yield point the friction stress at the point of contact with the channel wall remains constant. The significantly different character of the friction pairs of materials studied in [11] and those described above permits us to consider the new friction law valid for all cases of slippage of one (weaker) material over the surface of another (stronger) material.

3. In order to determine the true powder combustion law, an experimental study was made of the time dependence of pressure in a constant volume chamber with piezoelectric and crusher gauge pressure sensors installed.

The powder used in the experiments was in the form of cylindrical grains with seven channels and a double arch thickness of $0.4 \cdot 10^{-3}$ m. A typical pressure oscillogram is shown in Fig. 2 (p-axis, scale $0.79 \cdot 10^8$ N/m^2/division; t axis, 2.26 msec/division). Measurement uncertainty was not greater than 3% at an 0.9 confidence level. Divergence between indications of the piezoelectric and crusher sensors at maximum pressure did not exceed 4%.

In accordance with [9], the pressure oscillogram was used to obtain information on the actual process of gas formation during powder combustion in a closed volume. Using the maximum pressure values p_1^* and p_2^* for two different powder charge weights ω_1 and ω_2, the powder-gas covolume $\alpha = 1.1 \cdot 10^{-4}$ m^3/N and the powder force $f = 1.3 \cdot 10^5$ m were determined. The values $\omega_1 = 0.254$ N and $\omega_2 = 0.44$ N were chosen so that the values $p_1^* = 1.04 \cdot 10^8$ N/m^2 and $p_2^* = 1.91 \cdot 10^8$ N/m^2 corresponded to the pressure range in the ballistic apparatus powder chamber. In determining the values of p^*, the decrease in pressure produced by heat transfer to the chamber walls was considered. The values of α and f thus determined were then used to determine the dependence of relative weight fraction of combusted powder Ψ on time t and the function $\Gamma = \frac{1}{p}\frac{d\Psi}{dt}$, which describes the gas formation process. Figure 3 shows values of the function Γ, obtained for two different rarefaction densities $\omega/W_0 = 0.72 \cdot 10^3$ and $1.24 \cdot 10^3$ N/m^3 (points 1 and 2, respectively), where W_0 is the chamber volume. Although the powder grain form corresponds to a progressive combustion law, it is evident that the real combustion process occurs digressively. The function Γ can be approximated by

$$\Gamma = A_3 (1 - \Psi)^{A_4}, \tag{3.1}$$

where $A_3 = 0.41 \cdot 10^{-5}$ m^2/N·sec (curve 3), $A_3 = 0.35 \cdot 10^{-5}$ m^2/N·sec (curve 4), and $A_4 = 0.4$. Comparing Eq. (3.1) with the formula for a geometric powder-combustion law with a linear dependence of combustion rate on pressure $\Gamma = \varkappa\sigma_f/I$ (where $\varkappa$ is a constant dependent on grain form, σ_f is the relative area of the burning powder surface, and I is the total momentum of the powder gas pressure over the entire combustion time interval) we obtain $\sigma_f = (1 - \Psi)^{A_4}$, $A_3 = \varkappa/I$. From this it follows that for the real combustion process employed in the experiments with seven-channel powder, we can introduce an effective momentum value, which at $\varkappa = 0.72$ comprises $I = (0.175 - 0.205) \times 10^6$ H·sec/m^2. At the same time, the value of the total momentum obtained by integrating pressure over time comprises $0.53 \cdot 10^6$ N·sec/m^2 with an uncertainty not exceeding 8% at a confidence level of 0.9. This indicates the significant deviation of the real law of powder combustion in a closed volume from the geometric law.

4. In calculating the first stage of the ballistic apparatus, a diagram of which is presented in [1, 2], a gas formation law in the form of Eq. (3.1) was used. In addition it was assumed that $\omega/mg \leq 1$ (where m is the piston mass and g is the acceleration of free fall). This then permits use of the thermodynamic approximation [12].

The gasdynamic processes in the powder gases are described in dimensionless variables by the following system of equations:

$$\frac{d\Psi}{dt} = p(1 - \Psi)^{A_4}, \quad \frac{dp}{dt} = \begin{cases} \dfrac{h_1 \dfrac{d\Psi}{dt}\left[1 + (h_2 - h_3) h_1^{-1} p\right] - \gamma p v}{1 + x_1 - h_2\Psi - h_3(1 - \Psi)}, & \Psi < 1, \\ -\dfrac{\gamma p v}{1 + x_1 - h_2}, & \Psi = 1. \end{cases}$$

The piston motion for the case $p_1 < p_c$ and $p_2 = 0$ is described by Eq. (2.6), which in dimensionless variables has the form

$$v = dx_1/dt, \quad dv/dt = h_4 p k [\exp(4kl/d) - 1]^{-1}, \tag{4.2}$$

where, according to [5], $p_1 = p(1 + k_1\omega/mg)^{-1}$.

For $p_1 \geq \tau_c/k = p_c$, if we solve Eq. (2.10) for p_1 and differentiate the expression obtained with respect to time, with consideration of Eq. (4.1) we obtain

$$v = \frac{dx_1}{dt}, \quad a = \frac{dv}{dt}, \quad \frac{da}{dt} = \frac{h_7 a \dfrac{dp}{dt}(1 + k_1\omega/mg)^{-1}}{1 + h_6 a\left[h_5 - \ln(1 + 1/a h_6)\right]}. \tag{4.3}$$

The initial conditions for the system of equations (4.1), (4.2) have the form

$$t=0,\ x_1=0,\ v=0,\ p=p_f,\ \Psi=\frac{(1-h_3)(p_f-1)}{h_1+(h_2-h_3)(p_f-1)}. \tag{4.4}$$

For system (4.1), (4.3) for initial conditions we use the values of the dimensionless parameters obtained by solution of Eqs. (4.1), (4.2) for $p_1=p_c$.

In Eqs. (4.1)-(4.4) the following notation is used for the dimensionless quantities: p_0p, pressure; t_0t, time, x_1L_1, coordinate of back face of piston; vL_1/t_0, piston velocity; aL_1/t_0^2, piston acceleration; $t_0=(p_0A_5)^{-1}$; L_1, length of powder chamber; L_2, length of apparatus column; p_0, initial pressure in chamber; p_0p_f, drive pressure on piston; $p_0\tau_c$, maximum friction stress. Moreover, in these equations we have the dimensionless parameters

$$h_1=f\omega/p_0W_0,\ h_2=\alpha\omega/W_0,\ h_3=\dot{\omega}/\delta W_0,\ L_2/L_1,$$
$$h_4=\frac{4(1+k_1\omega/mg)^{-1}}{p_0L_1d\rho A_3^2},\quad h_5=bl,\quad h_6=\frac{\rho dL_1}{4t_0^2p_0\tau_c},\quad h_7=\frac{bd}{4\tau_c},$$

the adiabatic index of the powder gases γ and the coefficient $k_1=0.5$.

Numerical calculations performed on a computer for an experimental apparatus with a polyethylene piston ($L_1=0.432$ m; $L_2=5.45$ m, $d=0.034$ m; $l=0.228$ m, $m=0.204$ kg; $p_0=10^4$ N/m^2; $p_0p_f=5\cdot10^6$ N/m^2). The powder charge had the following values of constants: $\omega_1=0.98$ N; $\omega_2=1.22$ N; $\delta=0.157\cdot10^5$ N/m^3; $\gamma=1.2$; $\alpha=1.1\cdot10^{-4}$ m^3/N; $f=1.3\cdot10^5$ m; $A_3=0.41\cdot10^{-5}$ m^2/N·sec; $A_4=0.4$.

Table 1 presents the results of calculations of maximum powder gas pressure p* and piston muzzle velocity v* for various assumptions as to piston friction and powder combustion. Also shown are values of p* measured with the aid of the apparatus described in Section 3, and v* values measured by the photoelectric system of [13] with uncertainty not greater than 0.15%.

The calculated p* values obtained with the piston friction model developed above and the actual powder-combustion law differ from experiment by 3 and 19%. Since the pressure value is extremely sensitive to the form of the powder combustion and piston friction laws, such agreement between calculated and experimental p* values should be considered satisfactory. At the same time, the experimental v* values are 15 and 22% above the calculated ones. This is evidently related to the fact that the maximum value of friction stress decreases with increase in velocity. This affects the value of p* more weakly, since the maximum pressure in the gas is attained during the initial stage of piston motion (at $x_1L_1\simeq0.24$ m and $t_0t\simeq2.7\cdot10^{-}$ sec)*, while the velocity is still low. However, the presently available information on high velocity friction of polymers against steel [14] is insufficient for refinement of the ballistic apparatus calculations. This question will require special separate study.

With the actual powder-combustion law and the absence of friction, the calculated v* value is 23% higher than the experimental, while pressure is 2.0-2.3 times lower than that determined in experiment. These results show clearly that piston friction has a significant effect on the internal ballistics and must be considered in calculations.

To estimate the applicability of the geometric combustion law for a variable volume, a series of calculations were performed with consideration of friction at various values of I. The value $I=0.215\cdot10^6$ N·sec/m^2 (Table 1, row 3) was found to give the best agreement between experimental p* and v* values. This value differs greatly from the total momentum $I=0.53\cdot10^6$ N·sec/m^2, i.e., the geometric combustion law is not satisfied for the type of powder used in the experiments.

The authors express their gratitude to S. S. Grigoryan for his interest in the study and valuable advice, and to G. N. Suntsov for aid in performing the experimental studies.

LITERATURE CITED

1. S. Yu. Chernyavskii and N. N. Pilyugin, "Calculation of light gas ballistic apparatus parameters," Nauchn. Tr. Inst. Mekh. Mosk. Gos. Univ., No. 39, 73-92 (1975).
2. N. N. Pilyugin and S. Yu. Chernyavskii, "Calculation of gasdynamic parameters of a two-stage light gas ballistic apparatus with deformable piston," Izv. Akad. Nauk SSSR, Mekh. Zhidk. Gaza, No. 1, 69-75 (1976).
3. R. Piacesi, D. F. Gates, and A. E. Seigel, "Computer analysis of two-stage hypervelocity model launchers," in: Proceedings Sixth Symposium on Hypervelocity Impact, Vol. 1 (1963).

*As in Russian original— Consultants Bureau.

4. N. A. Zlatin, A. P. Krasil'shchikov, G. I. Mishin, and N. P. Popov, Ballistic Apparatus and Its Use in Experiment [in Russian], Nauka, Moscow (1974).
5. J. B. R. Murphy, L. K. Badhwar, and G. A. Lavoie, "Interior ballistics calculations systems for light gas guns and conventional guns," in: The Fluid Dynamics Aspects of Ballistics, AGARD Conf. Proc., No. 10 (1966).
6. G. L. Broad and J. Enstrom, "Interior ballistics, appearance of the flash, and the smoke cloud," in: Computer Calculation of Explosions [Russian translation], Mir, Moscow (1976).
7. L. Pennelezhen, "Microwave interferometer studies in shock tubes with a freely moving piston," in: Contemporary Technique in Aerodynamic Experiment at Hypersonic Velocity [in Russian], Mashinostroenie, Moscow (1965).
8. R. N. Teng, "Advances in light gas gun model-launching techniques," AIAA J., No. 11 (1967).
9. M. E. Serebryakov, Interior Ballistics of Column Systems and Powder Rockets [in Russian], Oborongiz, Moscow (1962).
10. C. B. Aibinder, K. I. Alksne, É. L. Tyunina, and M. G. Laka, Polymer Properties at High Pressures [in Russian], Khimiya, Moscow (1973).
11. S. S. Grigoryan and A. V. Ostroumov, "Mathematical modeling of snow avalanche motion," in: Reports of the International Conference on Glaciology, Cambridge [in Russian] (1976).
12. K. P. Stanyukovich, Transient Motions of a Continuous Medium [in Russian], Nauka, Moscow (1971).
13. S. Yu. Chernyavskii, "An apparatus used in a ballistic path to measure the velocity of flying models and synchronization," Prib. Tekh. Éksp., No. 3 (1976).
14. F. P. Bouden and D. Teibor, Friction and Lubrication of Solids [in Russian], Mashinostroenie, Moscow (1968).

STRUCTURE OF THE POTENTIAL BARRIER AT A METAL BOUNDARY

A. A. Porotnikov and B. B. Podnevich

UDC 537.581

In [1] the peculiarities of autoelectronic emission in an arc discharge plasma (F−P emission) connected with nonlinearity in the potential change in the precathode region were considered; it was shown that in the case where the negative electron charge density in the precathode layer can be neglected, the current density of F−P emission can differ by more than an order of magnitude from autoelectronic emission current density in a vacuum, as obtained with the Nordheim−Fowler expression. For the case where the precathode potential drop V_c is equal to the cathode work function φ, the modulus of the logarithm of the potential barrier transparency increases by 20% and the emission current density can decrease by a significant amount. An analogous change in current density can occur with other ratios between the quantities V_c and φ. In the present study we will consider these questions in greater detail for cases in which the negative space charge density cannot be neglected.

The potential distribution in the precathode region of an arc discharge can be obtained from the solution of the Poisson equation with the Langmuir−Macowan assumptions

$$\frac{dV}{dx}=\sqrt{16\pi j_i\left(\frac{MV_c^{1/2}}{2e}\right)\left\{\left(1-\frac{V}{V_c}\right)^{1/2}+q\left[\left(\frac{V}{V_c}\right)^{1/2}-1\right]\right\}},\tag{1}$$

where M is the atomic weight of the ion, e is the charge of the electron, j_i is the ion current density at the cathode, j_e is the electron current density at the cathode, $q=(j_e/j_i)\sqrt{m/M}$.

Following [1] we will consider two cases.

1. For $V_c \geq \varphi$ the expression for potential barrier transparency Q is written in the form

$$Q_{F-P}=\int_{x_1}^{x_2}\sqrt{\varphi-e/4x-V(x)}\,dx,\tag{2}$$

Moscow. Translated from Zhurnal Prikladnoi Mekhaniki i Tekhnicheskoi Fiziki, No. 5, pp. 80-86, September-October, 1978. Original article submitted October 3, 1977.